prevalence of nutritionally high-risk people for energy intake and each nutrient were estimated according to sex and age groups [7,8,13,25,26], using the ISU method [10,11]. Unfortunately, the ISU method is limited by large standard errors, when used to analyze small sample sizes, such as those for age-specific analysis. AGEVAR MODE would be more useful for small samples because of its smaller bias and lower standard errors.

Our study has some limitations. First, AGEVAR MODE assumes a monotonic change in both between-subject and within-subject variances, and does not deal with U- or J-shaped age variances. Therefore, AGEVAR MODE may not fit such data. However, such a situation is not likely to occur in actual situations, because dietary culture is passed from one generation to another. Second, we fitted 3 models to simulation data and actual data for sodium intake in women. To better assess the performance of the 3 methods, data for other nutrients need to be fitted and analyzed. Third, these 3 methods do not assume frequent zero intakes, even though the intake of foods such as bacon, cheese, and tomatoes can be zero on any given day. However, the intakes of nutrients such as sodium, fat, and protein in a day cannot be zero. Overall, we consider these 3 methods all now available for use in the analysis of nutrient intake.

Conclusions

Our improved method to estimate the usual intake distribution and the prevalence of nutritionally high-risk people showed good performance, when compared with the 2 existing modeling methods. This method will help promote the use of DRIs; help improve our understanding of the nutritional status among populations, and aid in confronting the challenges of public health nutrition.

Acknowledgment

The survey in this study was funded by project and research grants from the Ministry of Health, Labour and Welfare, Japan. The authors are grateful to the local healthcare staff in across Japan, especially the dieticians for collecting the dietary intake data.

References

1. Sasaki S (2008) Dietary Reference Intakes (DRIs) in Japan. Asia Pac J Clin Nutr 17: 420-444.
2. Subcommittee on Interpretation and Uses of Dietary Reference Intakes and the Standing Committee on the Scientific Evaluation of Dietary Reference Intakes (2003) Dietary reference intakes: applications in dietary planning. The National Academies Press, Washington DC, USA.
3. Cecil RL, Goldman L, Ausiello DA (2004) Nutrition in the prevention and treatment of disease, nutritional assessment: Cecil textbook of medicine. (22nd Edn), WB Saunders Company, Philadelphia, USA.
4. Yates AA, Schlicker SA, Suitor CW (1998) Dietary Reference Intakes: the new basis for recommendations for calcium and related nutrients, B vitamins, and choline. J Am Diet Assoc 98: 699-706.
5. Ross AC, Manson JE, Abrams SA, Aloia JF, Brannon PM, et al. (2011) The 2011 report on dietary reference intakes for calcium and vitamin D from the Institute of Medicine: what clinicians need to know. J Clin Endocrinol Metab 96: 53-58.
6. Guenther PM, Kott PS, Carriquiry AL (1997) Development of an approach for estimating usual nutrient intake distributions at the population level. J Nutr 127: 1106-1112.
7. Nakagawa Y, Daidai K, Ishikawa M, Yokoyama T (2012) Process evaluation of the dietary survey of plural days in the Health and Nutrition Survey in Kumamoto prefecture. J Natl Inst Public Health 61: 438-443.
8. Kobayashi M, Narumi M, Kanazaki M, Hanaoka S, Kobayashi Y (2012) Analysis in nagano prefecture health and nutrition survey. J Natl Inst Public Health 61: 430-437.
9. Subcommittee on Criteria for Dietary Evaluation CCoEoFCS, Food and Nutrition Board, National Research Council (1986) Nutrient adequacy: Assessment using food consumption surveys. National Academies Press, Washington DC, USA.
10. Nusser SM, Carriquiry AL, Dodd KW, Fuller WA (1996) A semiparametric transformation approach to estimating usual daily intake distributions. J Am Stat Assoc 91: 1440-1449.
11. Iowa State University (1996) A user's guide to C-SIDE (software for intake distribution estimation), version 1.0. Iowa State University, Iowa, USA.
12. Ministry of Health, Labour and Welfare (2012) Kokumin kenkou eiyou no genjou (Annual Report of the National Health and Nutrition Survey in Japan in 2009). Daiichi Publishing, Tokyo.
13. Nagano Prefecture J (2012)
14. Tochigi Prefecture J (2011).
15. Niigata Prefecture J (2010).
16. Waijers PM, Dekkers AL, Boer JM, Boshuizen HC, van Rossum CT (2006) The potential of AGE MODE, an age-dependent model, to estimate usual intakes and prevalences of inadequate intakes in a population. J Nutr 136: 2916-2920.
17. Waijers PMCM, Dekkers ALM, Boer JMA, van Rossum CTM (2007) Age dependent dietary assessment model (AGE MODE). Folate and vitamin A as examples. RIVM Report 1-92.
18. Ministry of Health, Labour and Welfare (2011) Kokumin kenkou eiyou no genjou (Annual Report of the National Health and Nutrition Survey in Japan in 2008). Daiichi Publishing, Tokyo.
19. Box GEP, Cox DR (1964) An analysis of transformations. J R Stat Soc Series B Stat Methodol 26: 211-252.
20. Dodd KW, Guenther PM, Freedman LS, Subar AF, Kipnis V, et al. (2006) Statistical methods for estimating usual intake of nutrients and foods: a review of the theory. J Am Diet Assoc 106: 1640-1650.
21. Ben-Israel A (1966) A Newton-Raphson method for the solution of systems of equations. J Math Anal Appl 15: 243-252.
22. Ypma TJ (1995) Historical development of the Newton-Raphson method. SIAM Review 37: 531-551.
23. Armitage P, Colton T (2005) Encyclopedia of biostatistics.
24. Ministry of Health, Labour and Welfare (2009) Dietary Reference Intakes for Japanese, 2010. Daiichi Publishing, Tokyo (in Japanese).
25. Saitama Prefecture (2012) Saitama Prefecture at a Glance.
26. Kumamoto Prefecture J (2012)
27. Ministry of Internal Affairs and Communications (2011) 2010 Population Census in Japan, Japan.
28. Ishiwaki A, Yokoyama T, Fujii H, Saito K, Nozue M, et al. (2007) A statistical approach for estimating the distribution of usual dietary intake to assess nutritionally at-risk populations based on the new Japanese Dietary Reference Intakes (DRIs). J Nutr Sci Vitaminol (Tokyo) 53: 337-344.
29. Resources Council of the Science and Technology Agency (2005) Standard Tables of Food Composition in Japan. (5th edn), Ministry of Finance Printing Bureau, Tokyo.
30. Ishikawa M, Yokoyama T (2012) Roles and issues of prefectural Health and Nutrition Survey for regional planning of Health Japan 21. J Natl Inst Public Health 61: 409-414.

Citation: Yokomichi H, Yokoyama T, Takahashi K, Yoshiike N, Yamagata Z (2013) An Improved Statistical Method to Estimate Usual Intake Distribution of Nutrients by Age Group. J Nutr Food Sci 3: 196. doi:10.4172/2155-9600.1000196

BIODOSIMETRY OF RESTORATION WORKERS FOR THE TOKYO ELECTRIC POWER COMPANY (TEPCO) FUKUSHIMA DAIICHI NUCLEAR POWER STATION ACCIDENT

Yumiko Suto,* Momoki Hirai,* Miho Akiyama,* Gen Kobashi,† Masanari Itokawa,‡ Makoto Akashi,§ and Nobuyuki Sugiura**

Abstract—**The biological dose of nuclear workers engaged in emergency response tasks at Tokyo Electric Power Company (TEPCO) Fukushima Daiichi Nuclear Power Station was estimated in the present study. As the national core center for radiation emergency medical preparedness in Japan, the National Institute of Radiological Sciences (NIRS) received all individuals who were suspected of being overexposed to acute radiation. In the course of health examinations at NIRS, biological dosimetry was performed by the dicentric chromosome assay (DCA). Twelve individuals were examined from 21 March–1 July 2011. The results indicated that the estimated exposure doses for all individuals were lower than 300 mGy, with the mean value of about 101 mGy. These results by DCA were in accordance with those obtained by physical dosimetry based on personal dosimeter recording assessment. The results corroborate the fact that no acute radiation syndrome was observed among the workers examined.**

Health Phys. 105(4):366–373; 2013

Key words: accident, nuclear; chromosome aberration; cytogenetics; dose assessment

INTRODUCTION

On 11 March 2011, the combined disaster of the Great East Japan Earthquake and subsequent tsunamis affected the Tokyo Electric Power Company (TEPCO) Fukushima Daiichi (1F) Nuclear Power Station (NPS). The NPS was seriously damaged, resulting in radioactive materials being released into the environment. The main event with the release of radioactive materials (^{131}I, ^{137}Cs, and ^{134}Cs, $\sim 10^{17}$ Bq in total) (Government of Japan 2011) into the atmosphere occurred during 12–15 March. On 12 April 2011, the Nuclear and Industrial Safety Agency (NISA) decided to raise the crisis level of the 1F NPS nuclear accident from the initial Level 5 to Level 7 (International Nuclear Event Scale: INES) based on the "People and Environment" criteria. Full information on the accident can be obtained from reports by the Japanese government (June 2011) (Government of Japan 2011) and TEPCO (June 2012) (TEPCO 2012a). Reportedly, a total of 3,754 workers, comprising the operational staff and emergency response personnel of TEPCO and its cooperative companies, were engaged in the restoration of the NPS at the 1F site from 11–31 March 2011. The evaluation of the status of workers' exposure dose was reported in due time in TEPCO's press releases (TEPCO 2012b).

Complying with requests from the Japanese government and TEPCO, staff members of the Research Center for Radiation Emergency Medicine of the National Institute of Radiological Sciences (NIRS) prepared for the medical care and dose assessment of radiation exposure for the restoration workers. The Center has been assigned as the National Center for Radiation Emergency Medical Preparedness and Response by the Nuclear Disaster Prevention Plan of the Japanese government since 1980 (NIRS 2011). For medical triaging and planning for radiation exposure patients, it is necessary to estimate the exposure dose of individual workers as soon as possible (IAEA 2001, 2011). Particularly at the initial stage of emergency work at the 1F site during March 2011, tsunamis deprived the system of radiation control measures and rendered many of the alarm personal dosimeters (APDs) and dose-reading devices unusable. Of a total of about 5,000 APD stockpiles, only 320 remained functional. Those usable APDs were shared among the workers until

*Department of Radiation Dosimetry, Research Center for Radiation Emergency Medicine, National Institute of Radiological Sciences, Chiba, Japan; †Research Center for Charged Particle Therapy, National Institute of Radiological Sciences, Chiba, Japan; ‡Department of Psychiatry and Behavioral Sciences, Tokyo Metropolitan Institute of Medical Science, Tokyo, Japan; §National Institute of Radiological Sciences, Chiba, Japan; **Radiation Environmental Effects Research Center, Nuclear Safety Research Association, Tokyo, Japan.

The authors declare no conflicts of interest.

For correspondence contact: Yumiko Suto, Biodosimetry Section, Department of Radiation Dosimetry, Research Center for Radiation Emergency Medicine, National Institute of Radiological Sciences (NIRS), 4-9-1 Anagawa, Inage-ku, Chiba-shi, 263-8555 Japan, or email at y-suto@nirs.go.jp.

(*Manuscript accepted* 26 *April* 2013)
0017-9078/13/0

DOI: 10.1097/HP.0b013e3182995e42

1 April. From 1 April 2011, all the workers were obliged to wear APDs according to the Ordinance on Prevention of Ionizing Radiation Hazards provided by the Ministry of Health, Labor and Welfare. This situation led the authors to consider that careful biological dosimetry was necessary to assess their individual exposure doses (IAEA 2001, 2011; ISO 2004), since they did not wear APDs during March 2011.

Thus, the Biodosimetry Section of NIRS decided to conduct the dicentric chromosome assay (DCA) for the workers who were suspected to be overexposed to radiation (Suto and Akashi 2011). The yield of dicentric chromosomes is considered to be a reliable, sensitive, and specific indicator of recent acute exposure to ionizing radiation (Vinnikov et al. 2010; IAEA 2011). In DCA, the frequency of dicentrics per peripheral blood lymphocyte from a radiation-exposed individual is applied to a calibration curve (dose-response curve) that has been established by in vitro exposure experiments in advance (IAEA 2001, 2011; ISO 2004). NIRS gave the highest priority to the workers to be examined: any of (a) those who were suspected to be exposed to doses greater than 1 Gy or (b) those who were exposed to an uncertain level of doses caused by mishandling or unusable conditions of APDs. The official members of the NIRS Chromosome Network Council (NIRS 2011), consisting of eight other laboratories in Japan (H. Tatsuno of Asahikawa Medical College, M. Yoshida of Hirosaki University, K. Tanaka of Institute for Environmental Sciences, S. Sonta of Human Science Center, S. Kodama of Osaka Prefecture University, T. Inaba of Hiroshima University, Y. Kodama of Radiation Effects Research Foundation, and T. Ikeuchi of Tokyo Medical and Dental University) stood by for extensive examinations when requested.

According to the above criteria, NIRS eventually received 12 workers by the end of July 2011 (2, 3, 2, 1, 1, 2, and 1 individuals on 21 March, 25 March, 30 May, 10 June, 20 June, 24 June, and 1 July, respectively) for biological dose assessment in conjunction with their health examinations. On 14 March 2011, under a special allowance from the NISA, the emergency dose limit was raised from 100 mSv y^{-1} to 250 mSv y^{-1} in effective dose. On 1 November 2011, the limit was lowered to 100 mSv y^{-1} for new emergency workers except in cases when they needed to respond to emergency situations, such as troubles arising at the water injection facilities for cooling nuclear reactors. From that time onward, the system of radiation control measures has been restored up until 31 January 2013. Therefore, NIRS has received no further individuals who require dose assessment or medical treatment since 30 July 2011. At NIRS, periodical health examinations have been conducted continuously in response to requests from those individuals and/or their doctors.

In this report, the current findings of biological dosimetry conducted for the individuals who were considered to be exposed to the highest dose of radiation among all workers at the 1F NPS site is described briefly.

MATERIALS AND METHODS

On 21 March 2011, two workers (Fu-1 and Fu-2) who were suspected of having been exposed to uncertain levels of radiation or greater than 1 Gy, were conveyed to this hospital, and DCA was performed using freshly drawn blood samples according to the IAEA manual (IAEA 2001). Subsequently on 25 March 2011, three workers were found to be exposed to radiation doses above 170 mSv estimated from ambient doses by the physical dosimetry-based measurements using APDs. Contamination from radioactive liquid (TEPCO 2011) on the skin of both feet was confirmed in two of them. Medical examinations showed that none of them had major systemic risks. The equivalent dose to the skin of the feet (i.e., partial exposure to the skin) was initially estimated to be 2–6 Sv from the concentration of radionuclides and the duration of time that the workers' feet were soaked in the contaminated water (<1 h), but this was later revealed to be lower (1.06–1.28 Sv).

Although medical diagnostic tests indicated that no specific treatment was needed, they were hospitalized for follow-up and discharged without any health problems on 28 March 2011. Seven workers who worked in the 1F plant inside or outside of buildings exhibited a high level of whole body counter (WBC) value (internal dose) according to the physical dose assessment conducted by the Japan Atomic Energy Agency (JAEA). These workers came to NIRS from 30 May to 1 July 2011. Some of them did not wear facemasks properly while they worked in the 1F. Internal contamination was determined to be mainly ^{131}I. The committed effective dose from internal contamination was up to 590 mSv. Their state of health was followed in the outpatient clinic of this institute. The radioactivity in their thyroid glands due to internal contamination decreased rapidly as expected.

As a result, blood samples obtained from 12 nuclear plant workers of the 1F NPS for biological dosimetry were examined from 21 March to 1 July 2011 (Table 1). Since 2 July 2011, no new workers have been subjected to biological dosimetry because no accidental exposure occurred at the NPS.

The present DCA was approved by the research ethics committee for NIRS (Registration Nos. 05-002, 11-011, and 11-025). All data recorded in their medical charts were used in the present research. The sample questionnaire shown in Annex B in ISO 19238 (2004), which includes questions about each worker's occupational and medical exposure history and smoking habit, was filled in by the

Table 1. Information of restoration workers for the Fukushima Daiichi Nuclear Power Station accident examined by the dicentric chromosome assay (DCA).

ID	Age	Sex	ARS and other symptoms[a]	Smoking (pieces per day)	Working history before 11 March 2011	Medical history of radiation exposure (last 15 y)
Fu-3	27	male	(−)	10 – 20	3 – 4 y (~ 0 mSv)	X-ray[b]
Fu-4	34	male	(−)	0	12 y (< 0.4 mSv)	X-ray[b]
Fu-5	32	male	(−)	30 – 40	14 y (< 0.2 mSv)	X-ray[b]
Fu-6	38	male	(−)	15	no record	X-ray[b]
Fu-7	43	male	(−)	0	no record	X-ray[b]
Fu-8	52	male	(−)	0	34 y	X-ray[b]
Fu-9	28	male	(−)	0	no record	X-ray[b]
Fu-10	24	male	(−)	0	6 y	X-ray[b]
Fu-11	20	male	(−)	0	3 y	X-ray[b]
Fu-12	34	male	(−)	0	no answer	X-ray[b]

[a]Acute radiation syndrome (ARS) and other clinical symptoms associated with radiation exposure are described.
[b]These x-ray exposures were performed as annual health checkups.

workers. Full informed consent was obtained from 10 of 12 workers; two workers gave informed consent with respect to the cytogenetic examinations, but they withheld consent for their detailed personal data to be published. NIRS staff agreed with the informed consent with reservations, and accordingly the results of DCA on the two individuals were handled separately in this study.

To assure sufficient metaphase spreads to be scored, the following two experimental procedures of 48-h peripheral blood lymphocyte culture [48-h treatment of colcemid (0.05 μg mL^{-1}) (culture-A) and final 2.5-h treatment of colcemid (0.5 μg mL^{-1}) (culture-B)] were conducted. Heparinized peripheral blood was collected from each individual, and mononuclear blood cells were isolated by using BD Vacutainer CPT tubes (BD Biosciences, San Jose, CA) according to the manufacturer's instruction. Cells were suspended in RPMI 1640 medium (approximately 1×10^6 cells mL^{-1}) containing HEPES buffer (Life Technologies, Carlsbad, CA), 20% fetal bovine serum (SAFC Biosciences, Lenexa, KS), 2% phytohaemagglutinin-HA15 (Remel, Lenexa, KS), and 100 μg mL^{-1} of kanamycin solution (Life Technologies) in a 15-mL Falcon tube. As for culture-B, each mononuclear cell suspension was divided into two equal parts. One part was cultured with the addition of 5-bromo-2′-deoxyuridine (BrdU) (Sigma-Aldrich, St. Louis, MO) (9 μg mL^{-1}) from the initiation of culture (culture B-1) and the other without the addition of BrdU (culture B-2). After 48-h culture, cells were harvested, treated with 0.075 M KCl, and fixed with methanol/acetic acid (3:1) according to the standard cytogenetic procedure (IAEA 2001, 2011). Then the air-dried chromosome preparations were stained with Giemsa (Merck Millipore, Billerica, MA).

Soon after completing chromosome preparations, Giemsa-stained metaphase images were captured in the AutoCapt mode by using two sets of AXIO Imager Z2 (Carl Zeiss AG, Oberkochen, Germany) equipped with CCD cameras and Metafer 4 software (MetaSystems GmbH, Altlussheim, Germany). Then metaphases for scoring were selected in a manual mode. Using these selected metaphase images, manual full dicentric scoring was performed. Other chromosome- or chromatid-type aberrations, such as rings, acentric fragments, and chromatid exchanges, were also recorded. Metaphases with less than 45 centromeres were omitted from the data. Three investigators started to examine 50 metaphases per slide according to the IAEA manual (IAEA 2001) and ISO 19238 (ISO 2004). If one or more than one dicentric chromosomes were detected, then they continued to score 50 more metaphases. The results derived from 50 or 100 metaphase analyses were reported to the physicians in charge of radiation emergency medicine. This procedure was completed in 2–3 h after chromosome slide preparations. Cell proliferation kinetics was assessed in preparations from B-1 cultures by sister-chromatid differentiation (SCD) patterns revealed by fluorescence plus Giemsa (FPG) staining (IAEA 2001, 2011). Cells at the first and second mitosis were scored for at least 200 metaphases. When the second metaphases did not exceed 5%, it was presumed that the parallel and simultaneous cultures (cultures B-2) had the same proportion of second metaphases as the B-1 cultures, and therefore conventionally stained preparations from B-2 cultures were scored. When the frequency of second metaphases exceeded 5%, dicentrics in A-cultures were scored. Alternatively, it was possible to score first metaphases exclusively in the chromosome preparations from B-1 cultures, but B-1 preparations were not used. This was because the first metaphases often looked fuzzy due probably to the heat treatment in the FPG procedures for differential staining, resulting in an inaccurate dicentric scoring. The initial triage stage of reporting was followed by full analysis according to the IAEA manual (IAEA 2001); 1,000 metaphases or more were analyzed. These dicentric assessment procedures were completed in two days. Then, the results of metaphase scoring and dose estimates were uploaded to the NIRS hospital database. The physicians explained the results to the donors at the second medical consultation held in a week.

The control level of dicentric chromosome yields for 14 age-matched and occupationally non-exposed healthy volunteers (age range: 22–59, five males and nine females) was also investigated. The dose response curve was established for blood cultures from a healthy nonsmoking adult female. To estimate doses, calculation software CABAS 2.0 (Deperas et al. 2007) was used by applying a linear-quadratic equation to the dose-effect curve, $Y = A + aD + bD^2$ (Y: the yield of dicentrics, D: the dose, A: the background frequency, a: the linear coefficient, b: the dose squared coefficient) (IAEA 2011), with the coefficients $A = 0.00015 \pm 0.00017$, $a = 0.0302 \pm 0.0044$, $b = 0.0588 \pm 0.0028$ ($\chi^2 = 5.24$, $p = 0.73$), which were established from ^{60}Co irradiation in vitro at 11 dose points (0, 0.1, 0.25, 0.5, 0.75, 1, 1.5, 2, 3, 4, and 5 Gy) at a dose rate of 0.5 Gy min^{-1} (Table 2, Fig. 1).

RESULTS

During the initial 50-metaphase scoring procedure, no individual showed dicentric chromosomes. Therefore, the authors proceeded to the next step of analyzing 1,000 metaphases or more. Metaphase chromosomes from B-2 cultures were examined for all but two individuals (Fu-9 and Fu-12) whose chromosome preparations obtained from B-1 cultures showed a high proportion of second metaphases (15.0% and 20.2%, respectively). For the two individuals showing a rapid cell proliferation rate, dicentrics in chromosome preparations obtained from A cultures were scored. The results of DCA are summarized in Table 3. The detailed personal data on two workers (Fu-1 and Fu-2) were not included in the table due to their reservations regarding informed consent described above. None of the remaining 10 workers had a history of medical exposure such as a computed tomography (CT) scan, which was reported to increase the frequency of dicentric chromosomes (Lee et al. 2012). Background dicentric frequencies obtained from the 14 control samples (aged 22–59) were 0 (11 donors), 1 (two donors), and 2 (one donor) per 1,000 cells.

Table 2. Dose-response curve data for the dicentric chromosome assay (DCA).

Dose (Gy)	No. of cells	Dicentric equivalent counts[a]	Yield	V/m[b]
0	5,000	1	0.0002	1
0.1	5,003	11	0.0022	1.180
0.25	2,606	30	0.0115	0.989
0.5	2,107	68	0.0323	0.968
0.75	1,674	101	0.0603	0.980
1	1,112	102	0.0917	0.968
1.5	720	129	0.1792	0.993
2	415	128	0.3084	0.897
3	277	162	0.5848	0.776
4	117	122	1.0427	0.866
5	245	394	1.6082	0.816

[a]The number of centromeres minus one in a multi-centric chromosome equals dicentric equivalent count.
[b]Variance to mean ratio. The p values of goodness of fit test for the Poisson distribution at every dose point where $p > 0.05$, except for 0.1-Gy dose point ($p < 0.05$) at which one cell possessing two dicentrics was unexpectedly observed.

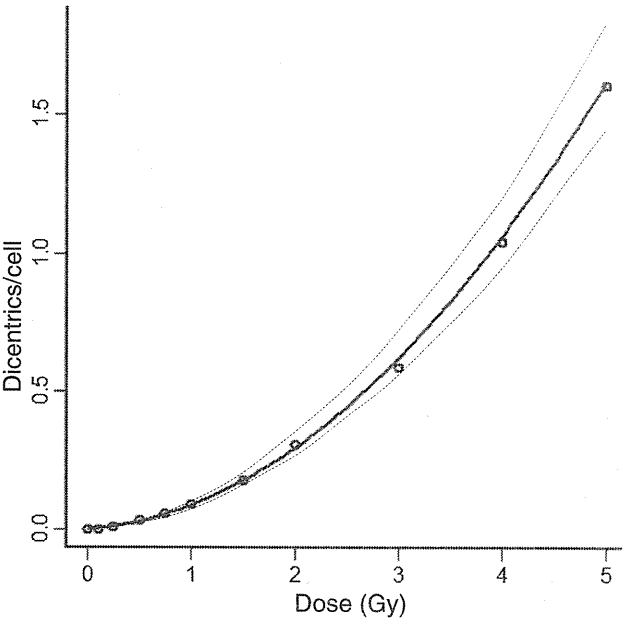

Fig. 1. Dose-response curve for the dicentric chromosome assay (DCA). $Y = (0.00015 \pm 0.00017) + (0.0302 \pm 0.0044) \times D + (0.0588 \pm 0.0028) \times D^2$; Y: dicentric yield, D: dose (Gy); p value of goodness of fit test : $p = 0.73$. Dotted lines denote 95% confidence limits.

As shown in Table 3, the estimated doses based on the frequencies of dicentrics (expressed as dicentric equivalent counts per cell) in 10 workers ranged from 26–171 mGy by using the calibration formula for DCA established at NIRS. The maximum value was obtained for Fu-4, whose personal physical estimate was 180 mSv. Fig. 2 illustrates the relationship between biological and physical dose estimates of the workers. The following linear regression was obtained:

$$[\text{physical dose (mSv)}] = [\text{biological dose (mGy)}] \times [1.03 \pm 0.33] - [7.07 \pm 37.70] \; (p < 0.05). \quad (1)$$

Centric ring chromosomes, which are radiation-specific chromosome markers, were detected in four workers (Fu-6, Fu-7, Fu-8, and Fu-10). A poor correlation was found between the yield of dicentrics and the age of subjects among the workers and controls; the values of coefficient of determination (R^2) were 0.001 and 0.048, respectively.

DISCUSSION

Biological dose estimation by dicentric chromosome analysis

DCA has been used as a reliable method for biological dose assessment in previous serious radiation accidents,

Table 3. Results of biological dosimetry of restoration workers for the Fukushima Daiichi Nuclear Power Station accident examined by the dicentric chromosome assay (DCA) and records of physical dosimetry detected with alarm personal dosimeters (APDs).

ID[a]	APD record (mSv)[a]	No. of metaphases scored	Dicentric equivalent counts (DIC)[b]	DIC per metaphase	Dose estimated by DCA (mGy)	95% LCL[c] (mGy)	95% UCL[d] (mGy)
Fu-3	179	1,003	7	0.00698	170	77	298
Fu-4	180	1,000	7	0.00700	171	77	299
Fu-5	173	1,000	5	0.00500	129	45	255
Fu-6	87	1,036	1	0.00097	26	0	137
Fu-7	38	1,005	4	0.00398	105	29	230
Fu-8	102	1,013	4	0.00395	105	29	229
Fu-9	unknown	1,035	6	0.00580	146	59	271
Fu-10	17	1,037	3	0.00289	79	14	199
Fu-11	4	1,042	1	0.00096	26	0	136
Fu-12	unknown	1,004	2	0.00199	55	3	174

[a]Detailed data and information of the alarm personal dosimeter (APD) record of each worker will be published elsewhere.
[b]The number of centromeres minus one in a multi-centric chromosome equals dicentric equivalent count.
[c]Lower confidence limit.
[d]Upper confidence limit.

such as the Chernobyl accident in 1986, (UNSCEAR 2000; Sevan'kaev et al. 2005), the Goiânia accident in 1987 (Ramalho et al. 1998), the JCO criticality accident in 1999 (Sasaki et al. 2001), and the Bulgaria accident in 2011 (Grégoire et al. 2013). In the present study, DCA was confirmed to be a powerful tool for medical triaging in the Fukushima NPS accident, particularly with the help of an automated detection system with metaphase-finding and image-capturing functions. Since the maximum equivalent dose (mainly ^{131}I, ^{134}Cs, and ^{137}Cs) of internal exposure among the 12 workers was estimated to be less than 1 mSv, the yield of dicentrics was considered to be caused by their external exposure.

Immediately after being informed of the TEPCO accident, NIRS prepared for triage treatments and dose estimation. The Biodosimetry Section of NIRS continued to analyze emergency situations under such unusual circumstances by gathering flash information released by the government. The physical dose assessment of the site workers performed immediately after the accident suggested that serious overexposure to workers could be avoided. However, to deal with the possibility of mass casualties, equipment and reagents required to conduct at least 200 cultures were prepared.

The present DCA eventually indicated that, in agreement with the abovementioned physical dose assessment, there was no serious overexposure case. A total of 12 workers came to the institute after the accident. As shown in Table 3, no individuals, including those whose personal data were not given, showed values exceeding the dose limit of 250 mGy. When considering a 95% confidence limit of dose estimates based on approximately 1,000 metaphases per donor, the value was below 300 mGy, which is lower than the lower limit level of medical triage for acute radiation syndrome (ARS) (1 Gy). The average dicentric yield per cell for a total of 10 individuals was 3.95 ± 2.26 per 1,000 cells. This value is not significantly different from that for the nuclear plant workers reported previously by Lloyd et al. (3.7 ± 0.5 per 1,000 cells) (1980).

The authors were deliberate in dealing with the dose estimation values obtained from DCA; they were waiting for different types of estimation results to be accumulated. The chromosome analysis indicated that the estimated physical and biological doses were in good agreement. Since the first examinations were conducted in NIRS in 2011, no individuals exhibiting signs of ill health due to the effects of exposure were reported among onsite

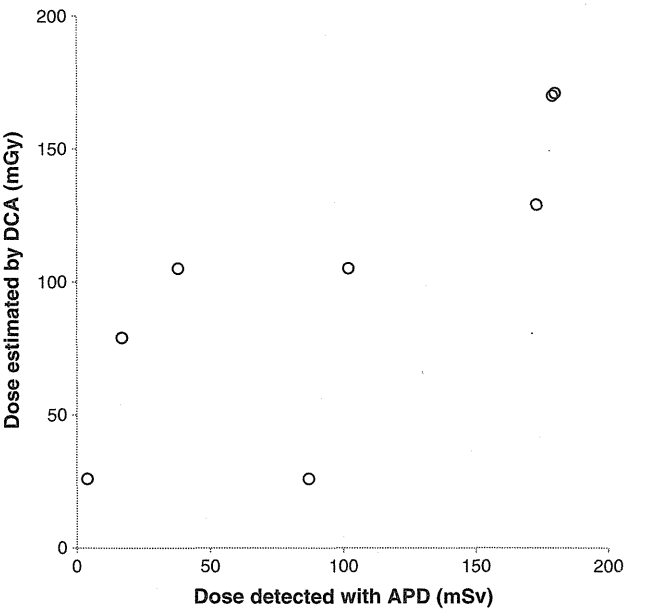

Fig. 2. Correlation between physical doses detected with alarm personal dosimeters (APDs) and biological doses estimated by the dicentric chromosome assay (DCA). The following linear regression was obtained: [physical dose (mSv)] = [biological dose (mGy)] × $[1.03 \pm 0.33] - [7.07 \pm 37.70]$ ($p < 0.05$).

workers. About a year later, the chromosomes of six out of 10 individuals were reexamined as a part of their annual health examinations (29 July–6 August 2012). As expected, no significant variation from the first estimates was observed in any of the donors; every individual showed either a decreasing tendency or the same results obtained from the former examinations (data not shown). Further examinations for the remaining four individuals are expected.

Interestingly, as shown in Fig. 2, there seems to be a close correlation between physical and biological dose estimates, suggesting that actual physical doses could be estimated by DCA even in cases of exposure to less than 250 mGy radiation. However, there remain uncertainties in the estimated biological doses, particularly in the estimated dose range below 100 mGy, based on the small number of cells examined. In addition, complicated factors possibly affecting the yield of dicentrics should be taken into consideration. It is unclear to what extent the induction of dicentrics in their past irradiation history might contribute to the present-day yields of dicentrics. Most individuals had been engaged in nuclear power plant work for a certain period. Therefore, it is reasonable to consider that the dicentric yields detected in the present study are the cumulative ones induced at the current accident and past potential radiation exposures, since the half-life of the persistence of dicentrics was estimated to be about 3 y (Buckton et al. 1978). Furthermore, some individuals were smokers, and some of the individuals reported an alcohol drinking habit. It is unclear to what extent these factors had a synergetic effect on the yield of dicentrics with the exposure at the 1F site.

Analysis of cumulative cytogenetic dose effects is ongoing in this institute by the multiplex fluorescence in situ hybridization (M-FISH) method to detect a stable type of chromosome aberration (translocation) (IAEA 2011; Suto et al. 2012a). From preliminary M-FISH analysis for 200–300 cells per donor thus far examined, it is suggested that the frequency of translocations is higher in the workers than in the control group (data not shown). This may be a clue for estimating cumulative doses.

Lessons learned from Fukushima Daiichi NPS accident in terms of biodosimetry

The Fukushima accident far exceeded the authors' expectations, due to the double disasters that damaged the nuclear power plant. They want to share the information gained from this accident, particularly regarding what they experienced in the course of biodosimetry. As a mission of NIRS, the research section was ready for any type of radiation-related casualty. This time, a nuclear accident and disaster caused by large earthquakes covering a wide area of Japan occurred. The transportation system was paralyzed, and the supply of electricity stopped for hours. Moreover, laboratories and suppliers of experimental reagents were damaged in Tohoku district. No overexposure that caused immediate harm to health, such as ARS, was detected during that period.

In this case, the number of samples to be examined was small, and therefore, the poor transportation conditions caused by the accident did not affect mission performance. Assuming that a large number of samples had to be dealt with, the poor transportation conditions would have caused problems in executing DCA. In addition, some facilities for sample collection inside the restricted area were difficult to access. As a lesson learned from this case, a complete backup system with surplus materials should be established to prepare for the worst-case scenario.

An optimal cell culture protocol should be established in advance. To perform DCA in such an emergency scene as the present case, two technical requirements should be satisfied: speed and accuracy. These are often conflicting requirements. In the present case, there was time to conduct dual cell culture procedures. The 48-h treatment of colcemid promised a high yield of first metaphases. However, the metaphase cell population contained highly contracted as well as highly elongated chromosomes because of the long-term treatment with a low concentration of colcemid. As a result of automated metaphase capturing, the subsequent procedure for selecting metaphases appropriate for analysis by manual mode became complicated and time consuming. On the other hand, cultures with 2.5-h colcemid treatment gave a high yield of metaphase spreads that were easy to analyze, although a certain proportion of metaphases was in the second mitosis. Individual differences in the cell proliferation kinetics should be taken into consideration to obtain appropriate chromosome preparations for efficient scoring. From the authors' experience, the frequency of second metaphases in 48-h cultures was at most 5% for adults. In the present experiments, however, two individuals (Fu-9 and Fu-12) showed an exceptionally high proportion of second metaphases (15.0% and 20.2%, respectively). Blood samples from children exhibit a rapid proliferation rate under the same culture conditions as those for adults. Supposing that exposed populations included young people, differences in cell proliferation kinetics would have influenced the efficiency of the detection of metaphases suitable for accurate scoring of dicentrics. Note that dose response relations have been established for adults, not for the young. Further information that is related to the biological dosimetry by DCA, such as the radiation sensitivity in the young, is necessary for the accurate dose assessment of radiation.

A rapid and sensitive fluorescence in situ hybridization method using peptide nucleic acid probes (PNA-FISH) for centromeric and telomeric repeat sequences was proposed as an alternative methodology that detects

dicentrics accurately (Shi et al. 2012). For conducting large-scale biodosimetric examinations, DCA using the automated scoring (IAEA 2012; Vaurijoux 2009, 2012) of PNA signals would be very useful. However, preliminary performance of PNA-FISH proved to be inefficient for detecting dicentrics in practice (Suto et al. 2012b). Fluorescent images obtained by this method required computer-aided processing to generate distinct centromere signals under the experimental conditions. The development of sophisticated software specific for the image analysis of PNA-FISH is necessary.

Health management should be conducted even after the resignation of the nuclear power plant workers. For the purpose of long-term health management, a database has been constructed at NIRS to track the radiation doses and to control the working regulations for the workers involved in emergency tasks at the TEPCO Fukushima Daiichi Nuclear Power Station. As mentioned earlier, dicentric yields detected in blood samples from workers may be caused by cumulative exposure during their nuclear jobs. To cope with these complicated issues with respect to the assurance of their health management, the establishment of certain guidelines is necessary.

In conclusion, the DCA indicates that the estimated exposure doses for 10 workers who were suspected to be overexposed during the restoration work did not exceed 300 mGy. The DCA was confirmed to be a powerful and rapid tool for medical triaging in the Fukushima NPS accident with the aid of an automated cytogenetic imaging system. Estimated values were in agreement with those of physically estimated doses. On this occasion, the need for improved cytogenetic research strategies adopted for mass-casualty management was reconsidered.

Acknowledgments—We would like to express our sincere appreciation to Carl Zeiss Microscopy Co., Ltd. (Tokyo, Japan) and MetaSystems Asia Co., Ltd. (Hong Kong, China) for the support of our activities in response to the TEPCO Fukushima Daiichi Nuclear Power Station accident. We would like to thank David Lloyd, Firouz Darroudi, and Toshikazu Suzuki for their advice and information. Lastly, we are grateful to many domestic and international investigators for their offers of help extended to us.

REFERENCES

Buckton KE, Harilton GE, Paton L, Langlois AO. Chromosome aberrations in irradiated ankylosing spondylitis patients. In: Evans HJ, Lloyd DC, eds. Mutagen-induced chromosome damage in man. London: London University Press; 1978: 142–150.

Deperas J, Szluinska M, Deperas-Kaminska M, Edwards A, Lloyd D, Lindholm C, Romm H, Roy L, Moss R, Morand J, Wojcik A. CABAS: a freely available PC program for fitting calibration curves in chromosome aberration dosimetry. Radiat Protect Dosim 124:115–123; 2007.

Government of Japan (Nuclear Emergency Response Headquarters), Report of the Japanese Government to the IAEA Ministerial Conference on Nuclear Safety—the accident at TEPCO's Fukushima Nuclear Power Stations; 2011. Available at ***www.kantei.go.jp/foreign/kan/topics/201106/iaea_houkokusho_e.html***. Accessed 18 June 2011.

Grégoire E, Hadjidekova V, Hristova R, Gruel G, Roch-Lefevre S, Voisin P, Staynova A, Deleva S, Ainsbury EA, Lloyd DC, Barquinero JF. Biological dosimetry assessments of a serious radiation accident in Bulgaria in 2011. Radiat Protect Dosim 155: 418–422; 2013.

International Atomic Energy Agency. Cytogenetic analysis for radiation dose assessment. A manual. Vienna: IAEA Publications; Technical Report Series No. 405; 2001.

International Atomic Energy Agency. Cytogenetic dosimetry: applications in preparedness for and response to radiation emergencies. Vienna: IAEA Publications; 2011.

International Organization for Standardization. ISO 19238: radiological protection—performance criteria for service laboratories performing biological dosimetry by cytogenetics. Geneva: ISO; TC 85/SC 2; 2004.

Lee JK, Han EA, Lee SS, Ha WH, Barquinero JF, Lee HR, Cho MS. Cytogenetic biodosimetry for Fukushima travelers after the nuclear power plant accident: no evidence of enhanced yield of dicentrics. J Radiat Res 5:876–881; 2012.

Lloyd DC, Purrott RJ, Reeder EJ. The Incidence of unstable chromosome aberrations in peripheral blood lymphocytes from unirradiated and occupationally exposed people. Mutation Res 72:523–532; 1980.

National Institute of Radiological Sciences. Research Center for Radiation Emergency Medicine: overview. Annual Report: April 2010–March 2011. Chiba, Japan: NIRS; 2011: 69–70. Also available at ***www.nirs.go.jp/publication/annual_reports_en/pdf/2010/full.pdf***. Accessed 12 February 2013.

Ramalho AT, Costa ML, Oliveira MS. Conventional radiation-biological dosimetry using frequencies of unstable chromosome aberrations. Mutat Res 404:97–100; 1998.

Sasaki MS, Hayata I, Kamada N, Kodama Y, Kodama S. Chromosome aberration analysis in persons exposed to low-level radiation from the JCO criticality accident in Tokaimura. J Radiat Res 42:Suppl:S107–S116; 2001.

Sevan'kaev AV, Llloyd DC, Edwards AA, Khvostunov IK, Mikhailova GF, Golub EV, Shepel NN, Nadejina NM, Galstian IA, Nugis VY, Barrios I, Caballin MR, Barquinero JF. A cytogenetic follow-up of some highly irradiated victims of the Chernobyl accident. Radiat Prot Dosim 113:152–161; 2005.

Shi L, Fujioka K, Sun J, Kinomura A, Inaba T, Ikura T, Ohtaki M, Yoshida M, Kodama Y, Livingston GK, Kamiya K, Tashiro S. A modified system for analyzing ionizing radiation-induced chromosome abnormalities. Radiat Res 177:533–538; 2012.

Suto Y, Akashi M. REMPAN response to Fukushima—biodosimetry for workers at Fukushima Nuclear Power Station. REMPAN e-Newsletter 3: 2; 2011. Würzburg, Germany: Radiation Emergency Medical Preparedness and Assistance Network (REMPAN), World Health Organization (WHO); 2011. Available at: ***http://www.rempan.uk-wuerzburg.de/fileadmin/uk/rempan/Dokumente/WHO_REMPAN_e-Newsletter_-_Issue_3_-_July_2011.pdf***. Accessed 1 July 2011.

Suto Y, Hirai M, Akiyama M, Yuki M, Nakagawa T, Tominaga T, Nakayama F, Suzuki T, Sugiura N. Induction and persistence of multicentric chromosomes in cultured human peripheral blood lymphocytes following high-dose gamma irradiation. Cytologia 77:347–358; 2012a.

Suto Y, Hirai M, Akiyama M, Suzuki T, Sugiura N. Sensitive and rapid detection of centromeric alphoid DNA in human metaphase chromosomes by PNA fluorescence in situ hybridization

and its application to biological radiation dosimetry. Cytologia 77:261–267; 2012b.

The Tokyo Electric Power Company (TEPCO), Press release: Result of the investigation on exposure to radiation of workers from cooperative companies at Unit3 in Fukushima Daiichi Nuclear Power Station (March 25, 2011); Available at ***www.tepco.co.jp/en/press/corp-com/release/11032503-e.html***. Accessed 25 March 2011.

TEPCO, Press release: Release of the Fukushima Nuclear Accidents Investigation Report; 2012a. Available at ***www.tepco.co.jp/en/press/corp-com/release/2012/1205638_1870.html.*** Accessed 20 June 2012.

TEPCO, Press release: exposure dose evaluation of the workers at Fukushima Daiichi Nuclear Power Station; 2012b. Available at ***www.tepco.co.jp/en/press/corp-com/release/2012/1211363_1870.html***. Accessed 31 July 2012.

United Nations Scientific Committee on the Effects of Atomic Radiation, UNSCEAR Report 2000, Vol. II, Annex J: exposures and effects of the Chernobyl accident; 2000. Available at ***www.unscear.org/docs/reports/annexj.pdf***. Accessed 12 February 2013.

Vaurijoux A, Gruel G, Pouzoulet F, Grégoire E, Martin C, Roch-Lefèvre S, Voisin P, Voisin P, Roy L. Strategy for population triage based on dicentric analysis. Radiat Res 171: 541–548; 2009.

Vaurijoux A, Gregoire E, Roch-Lefevre S, Voisin P, Martin C, Voisin P, Roy L, Gruel G. Detection of partial-body exposure to ionizing radiation by the automatic detection of dicentrics. Radiat Res 178:357–364; 2012.

Vinnikov VA, Ainsbury EA, Maznyk NA, Lloyd DC, Rothkamm K. Limitations associated with analysis of cytogenetic data for biological dosimetry. Radiat Res 174:403–414; 2010.

Cytologia **78**(1): 97–103

A Modified Protocol for Accurate Detection of Cell Fusion-Mediated Premature Chromosome Condensation in Human Peripheral Blood Lymphocytes

Yumiko Suto[1]*, Miho Akiyama[1], Takaya Gotoh[2], and Momoki Hirai[1]

[1] Department of Radiation Dosimetry, Research Center for Radiation Emergency Medicine, National Institute of Radiological Sciences, 4–9–1 Anagawa, Inage-ku, Chiba 263–8555, Japan
[2] Department of Radiation Emergency Medicine, Research Center for Radiation Emergency Medicine, National Institute of Radiological Sciences, 4–9–1 Anagawa, Inage-ku, Chiba 263–8555, Japan

Received October 10, 2012; accepted March 14, 2013

Summary When interphase cells are fused with mitotic cells, loosely distributing chromatins in nuclei are induced to form prematurely condensed chromosomes. In this paper we report a modified protocol to unequivocally detect prematurely condensed chromosomes in human peripheral blood lymphocytes that were fused with mitotic Chinese hamster ovary (CHO) cells. To examine cell fusion-mediated premature chromosome condensation (PCC), we conducted morphological analysis by differential interference contrast microscopy and molecular cytogenetic analysis by fluorescence *in situ* hybridization using pan-centromeric and telomeric peptide nucleic acid (PNA) probes. These modified procedures may serve to improve the usefulness of the technique of PCC in cytogenetic investigations.

Key words Premature chromosome condensation, Cell fusion, Radiation, PNA-FISH.

Premature chromosome condensation (PCC) is a phenomenon that occurs in eukaryotic interphase cells when they are fused with mitotic cells. The technique that induces PCC facilitates the visualization of interphase chromatin as a structure of condensed chromosome. The appearance of resulting prematurely condensed chromosomes varies depending on the cell-cycle position of the interphase at the time of PCC induction by cell fusion. While G0/G1 cells exhibit single-chromatid chromosomes, S cells show pulverized chromosomes and G2 cells yield elongated double-chromatid chromosomes. Studies on cell fusion-mediated PCC started in the early 1970s (Rao and Johnson 1970, Johnson and Rao 1970, Sperling and Rao 1974, Waldren and Johnson 1974). The search for substances that induce cell-fusion mediated PCC began, and a heterodimeric protein composed of cyclin B and cyclin-dependent kinase was identified as a substance that induces PCC (Nurse 1990, Freeman and Donoghue 1991). Since then, explorations for factors involved in cell cycle regulation have progressed greatly (Cheng *et al.* 1993). In the cells cycling in culture, inhibition of the DNA phosphorylation using Okadaic acid or calyculin A can also induce PCC (Pantelias and Maillie 1984, Durante *et al.* 1998, Prasanna *et al.* 2000, Gotoh *et al.* 2005, Gotoh 2009). This chemically induced PCC technique has been used for the analysis of the G2 PCC assay (Bezrookove *et al.* 2003, Kanda *et al.* 1999, Lamadrid *et al.* 2007, Lindholm *et al.* 2010). These PCC-inducing techniques enable analysis of the kinetics of chromatin formation in the early cell cycle stage (Rao *et al.* 1977).

* Corresponding author, e-mail: y-suto@nirs.go.jp.
DOI: 10.1508/cytologia.78.97

To analyze cytogenetic events occurring in human cells, peripheral blood lymphocytes (PBLs) are most commonly used in research. Chinese hamster ovary (CHO) cells exhibiting a distinctively different chromosomal constitution are used as mitosis inducer cells. PCC has been induced by cell fusion in the presence of fusing reagents, or fusogens, such as polyethylene glycol (PEG) (Pantelias and Maillie 1983). The cell fusion-mediated PCC technique has been used both in basic and applied cell sciences (Hittelman *et al.* 1979, Vyas *et al.* 1991, Garcia *et al.* 2001, Gotoh and Durante 2006, Stevens *et al.* 2010).

One especially significant application of this technique is the assessment of the genotoxicity of various reagents immediately following the induction of the primary DNA damage by visualizing chromosomes. In investigations on the biological effects of radiation, this technique is useful for exploring the immediate post-irradiation processes (Waldren and Johnson 1974, Pantelias and Maillie 1984, Vyas *et al.* 1991, Darroudi and Natarajan 1993, Blakely *et al.* 1995, Prasanna *et al.* 1997, Darroudi *et al.* 1998, Durante *et al.* 1998, Chambrette *et al.* 1999, Terzoudi and Pantelias 2006, Terzoudi *et al.* 2008, Pathak *et al.* 2009, Darroudi *et al.* 2010). The PCC assay allows analysis of the kinetics of chromosome aberration formation, which is eventually recognized as dicentrics, rings and translocations in the metaphase cells (Pantelias and Maillie 1985, Darroudi *et al.* 1998). Improved methods have been reported by combining conventional C-banding, centromere detection by fluorescence *in situ* hybridization (FISH) and chromosome painting (Hittelman *et al.* 1988, Evans *et al.* 1991, Pantelias *et al.* 1993, Durante *et al.* 1997, Prasanna *et al.* 2000, M'kacher *et al.* 2003, Prasanna and Blakely 2004, Darroudi *et al.* 2010). These improved methods permit the detection of chromosomal aberrations without the need for any culturing procedure. Therefore, the PCC assay has been proposed as a powerful biodosimetric tool in an internationally standardized technical report (International Atomic Energy Agency, IAEA) (IAEA 2001, 2011).

Although the cell fusion-mediated PCC assay has a wide range of potential applications, it has not been frequently utilized in cytogenetic researches compared to the chemically induced PCC assay. There were disadvantages in conducting the fusion-mediated PCC assay. One problem in the procedures for the PCC assay was that certain skills and experience were required to obtain fused cells efficiently. To solve this issue, improved methods have already been described in many references (IAEA 2011). The fuzzy appearance of prematurely condensed chromosomes poses another problem for accurate analysis of PCC. The prematurely condensed human chromosomes might also be confused with metaphase CHO chromosomes especially when the sister-chromatids of the CHO chromosomes are separated due to the excess effect of colcemid. Efforts have been made to find a way to overcome these problems concerning the difficulties in discerning between the chromosomes of two species. For instance, the 5-bromo-2′-deoxyuridine (BrdU) labeling technique has been used to differentially stain the chromosomes of mitosis inducer cells (Cornforth and Bedford 1983, Hittelman *et al.* 1988).

In this short technical report, we describe a newly modified protocol designed to accurately detect PCC in human PBLs.

Materials and methods

Cell fusion

A subclone of the CHO-K1 cell line, supplied from American Type Culture Collection (Summit Pharmaceuticals International Corporation, Tokyo, Japan), was used as the mitotic inducer for the PCC assay. The modal number of chromosomes in our CHO cells was 20. Mitotic CHO cells were harvested by the shake-off procedure 4–5 h after adding 0.1 μg/ml colcemid. Mitotic cells suspended in a cryopreservation medium (CELLBANKER, Zenoaq, Fukushima, Japan) (1×10^6 cells/ml) were poured in 1-ml vials and kept at −80°C until use. Blood samples were collected by venipuncuture in heparinized tubes from healthy donors after obtaining their informed consent.

Mononuclear cells, consisting of more than 90% lymphocytes, were isolated from whole peripheral blood using Ficoll-Hypaque sedimentation (Axis Shield, Oslo, Norway) and washed with medium RPMI-1640. Some of the isolated lymphocyte samples were exposed to 2-Gy gamma rays at a dose rate of 0.5 Gy/min to examine radiation-induced chromosome aberrations.

PCC was induced according to the procedure of IAEA (IAEA 2001, 2011). In brief, mitotic CHO cells were thawed to defreeze, suspended in medium RPMI-1640 and centrifuged for 7 min at 1,200 rpm. Then lymphocytes (5×10^6) and CHO cells (1×10^6) were mixed in a round-bottomed culture tube and washed again with RPMI-1640. After centrifugation (1,200 rpm, 7 min), the supernatant was discarded. Polyethylene glycol (PEG; 150 μl, 50% w/v, MW 1500) (Roche, Mannheim, Germany) was added onto the cell pellet and gently mixed. After a 1-min PEG treatment, 3 ml RPMI-1640 was added to dilute PEG and cells were washed. Subsequently 800 μl complete medium (90% RPMI-1640 and 10% fetal bovine serum) containing colcemid (final concentration: 150–200 ng/ml) was added and incubated for 1 h at 37°C. Hypotonic treatments with 0.075 M KCl and methanol–acetic acid (3 : 1, v/v) fixation were performed according to the standard chromosome preparation procedure.

Differential interference contrast microscopy

Air-dried chromosome preparations were weakly stained with 3% Giemsa solution (pH=6.8) for 3 min, instead of standard 25-min staining, and rinsed in clean water. These chromosomes were observed under a light microscope equipped with a differential interference contrast (DIC) apparatus (Olympus, Tokyo, Japan). The optical axis was adjusted to produce distinct images.

Fluorescence in situ hybridization

FISH using peptide nucleic acid (PNA) probes (PNA-FISH) was conducted as described previously (Suto *et al.* 2012), with modifications for PCC detection. Chromosome preparations were dried in an oven for 30 min at 64°C, fixed in 4% paraformaldehyde solution at 4°C for 2 min, followed by washing in phosphate buffered saline (PBS) and dehydration with an ethanol series. Then, chromosomes were denatured in an alkaline solution composed of 0.1 N NaOH (70%) and ethanol (30%) at room temperature for 40 s followed by dehydration in an ethanol series. Synthesized Cy3-conjugated pan-centromeric and carboxyfluorescein-aminohexyl (FAM)-conjugated telomeric PNA probes (Panagene, Daejon, South Korea) were used for chromosome identification. A total of 60 μl probe mix (60% formamide in 2×SSC, 5 ng salmon sperm DNA, 5 ng of each PNA probe) was denatured at 90°C for 5 min, dropped onto a slide to hybridize to alkaline-denatured chromosomes, covered with a piece of plastic film and kept at room temperature for 0.5–2 h in the dark. Then, the slide was washed in a post-hybridization solution (2×SSC/0.1% Tween-20) for 10 min at 57°C, air-dried, and counterstained with 125 ng/ml 4,6-diamidine-2-phenylindole (DAPI). When background noise was observed, the amount of each PNA probe was reduced to one fifth. For the analysis of fluorescent signals on chromosomes, images obtained from filter sets specific for DAPI, FITC and Cy3 were merged using image-processing software. Multiplex fluorescence *in situ* hybridization (M-FISH) was conducted using a commercially available multicolor probe (MetaSystems, Altlussheim, Germany) following the manufacturer's instructions with a slight modification. To economize on using the expensive commercially available probe, we diluted it to half of the recommended concentration with a hybridization buffer [50% formamide (v/v), 10% dextran sulfate (w/v) and 20% bovine serum albumin (v/v) in 2×SSC].

Results and discussion

The objective of this work was to modify the existing protocols for visualizing prematurely condensed chromosomes in human PBLs with accuracy. We present here a protocol with two-fold

modifications. For morphological analysis using conventionally stained chromosome preparations, we applied DIC microscopy to visualize the distinct shape of chromosomes. DIC microscopy enables us to analyze transparent biological objects without staining. DIC images give a relief-like appearance corresponding to the variation of the optical density of the object, emphasizing its outlines and edges. The resolution and clarity of images obtained by DIC microscopy are unsurpassed among other standard optical microscopy techniques. This optical feature worked well with weakly stained objects as represented in Fig. 1. Images produced by a DIC microscope seem to have a three-dimensional physical relief with a shadow cast. The distinct coil-shaped structure of interphase chromosomes was observed. This may facilitate further studies such as the analysis of chromosomal condensation and compaction in the course of cell-cycle progression in relation to DNA replication processes (Rao *et al.* 1977, Gotoh and Durante 2006, Gotoh 2007, 2009).

The feasibility of the present protocol was assessed in radiation dosimetry. In the analysis of

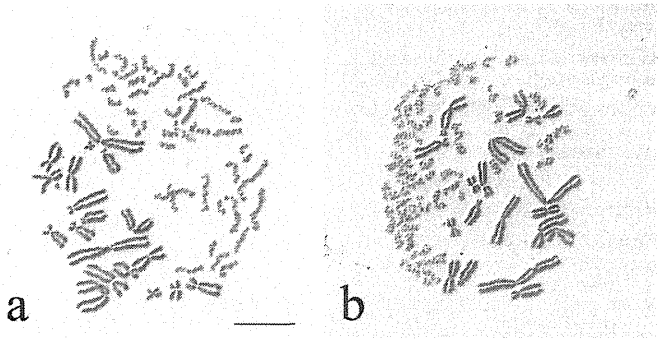

Fig. 1. Examples of cells showing fusion-mediated premature chromosome condensation (PCC). (a) Metaphase Chinese hamster ovary (CHO) chromosomes and prematurely condensed human chromosomes in a fused cell stained weakly with Giemsa solution. Chromosomes were viewed with a differential interference contrast (DIC) microscope. Metaphase CHO and prematurely condensed human chromosomes exhibited double and single-chromatid structure, respectively. (b) DIC image of less condensed human chromosomes. The coil structure of prematurely condensed chromosomes is clearly demonstrated. Scale bar=10 μm.

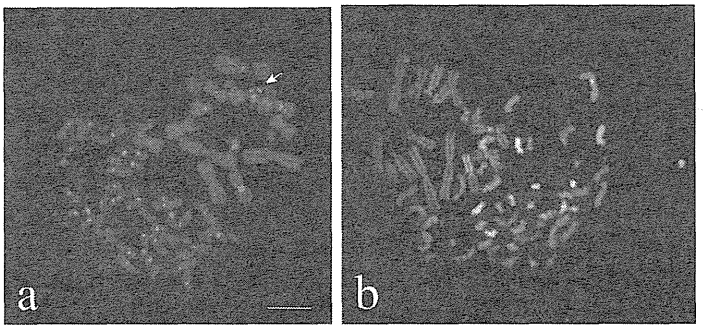

Fig. 2. Detection of prematurely condensed human chromosomes in fused cells by fluorescence *in situ* hybridization (FISH). (a) FISH with peptide nucleic acid probes (PNA-FISH) for pan-centromeric and telomeric repeat sequences. In this fused cell, all human chromosomes show centromeric alphoid signals (Cy3, red). Most CHO chromosomes exhibit hybridization signals with telomeric repeat sequences (FAM, green). Signals on amplified interstitial telomeric repeat sequences in CHO chromosomes are so intense that actual telomere signals on every chromosome are not displayed properly in this image. Note that the smallest chromosome in the CHO chromosomal complement can be identified because of its green hybridization signal (arrow). (b) Prematurely condensed human chromosomes in a fused cell identified by multicolor-FISH. This image was generated by merging separate images obtained with filters specific for the multicolor FISH probe. Scale bar=10 μm.

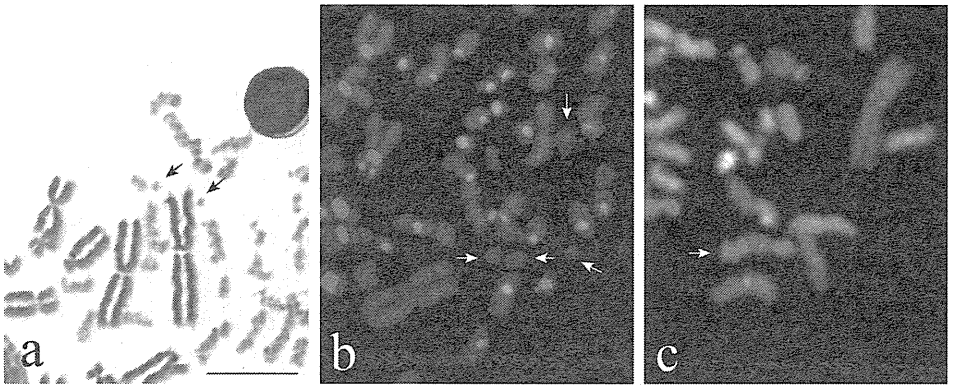

Fig. 3. Application of our modified protocol to the detection of radiation-induced chromosome aberrations in human interphase lymphocytes. (a) Radiation-induced fragments viewed with a DIC microscope (arrows). (b) Radiation-induced fragments examined by PNA-FISH. No centromeric signals were detected in acentric fragments (arrows). (c) A rearranged chromosome composed of three chromosome segments (arrow). Scale bar=10μm.

radiation-induced chromosome aberrations using conventionally stained preparations, the coiled substructure of prematurely condensed chromosomes often causes difficulty in identifying fragments, especially when uncoiled portions of chromosomes are seemingly unstained. Therefore, DIC microscopy may lead to the accurate scoring of radiation-induced fragments (Fig. 3a). For molecular cytogenetic analysis using pan-centromeric and telomeric PNA probes, we improved the accuracy of discrimination between human and CHO chromosomes based on the differential hybridization property of the two probes (Fig. 2a). The pan-centromeric alphoid DNA probe solely hybridized with human chromosomes. On the other hand, there were large blocks of hybridization sites with amplified telomeric repeat sequences (TTAGGG)n in CHO chromosomes (Slijepcevic *et al.* 1997, Bolzán *et al.* 2001). The smallest CHO chromosome, or chromosome 21 according to the standard karyotype of CHO-K1 (Xu *et al.* 2011), is likely to be confused with prematurely condensed human chromosomes by the conventional method. In our modified method, these chromosomes could be identified because of their marked hybridization signals (Fig. 2a). Therefore, PNA-FISH using pan-centromeric and telomeric probes enabled us to accurately count radiation induced chromosomal fragments in excess of background frequency by identifying fragments without centromeric signals (Fig. 3b).

We introduced M-FISH to the detection of prematurely condensed human chromosomes (Figs. 2b and 3c). The M-FISH enables information to be obtained on the chromosomal territory deduced from the relative location of chromosomes in G0/G1 phase. Commercially available M-FISH probes are expensive. We diluted probes with a hybridization mixture to half the recommended concentration, and obtained sufficient signal intensity. The continued development of the PCC technique will open new research avenues in cytogenetics. Our modified protocol presented here may serve as a powerful tool for examining interphase chromosomes.

Acknowledgements

The authors would like to thank Dr. F. Darroudi (Leiden University, The Netherlands) for his valuable and constructive suggestions. We are grateful to Ms. K. Tahara, Mr. T. Noda and Ms. M. Owaki for their technical assistance.

References

Bezrookove, V., Smits, R., Moestein, G., Fodde, R., Tanke, H. J., Raap, A. K., and Darroudi, F. 2003. Premature chromosome condensation revisited: a novel chemical approach permits efficient cytogenetic analysis of cancers. Genes Chromosomes Cancer **38**: 177–186.

Blakely, W. F., Prasanna, P. G. S., Kolanko, C. J., Pyle, M. D., Mosbrook, D. M., Loats, A. S., Rippeon, T. L., and Loats, H. 1995. Application of the premature chromosome condensation assay in simulated partial-body radiation exposures: evaluation of the use of an automated metaphase-finder. Stem Cells Suppl. **1**: S223–S230.

Bolzán, A. D., Páez, G. L., and Bianchi, M. S. 2001. FISH analysis of telomeric repeat sequences and their involvement in chromosomal aberrations induced by radiomimetic compounds in hamster cells. Mutat. Res. **479**: 187–196.

Chambrette, V., Laval, F., and Voisin, P. 1999. The utility of lymphocyte premature chromosome condensation analysis for biological dosimetry following accidental overexposure to ionizing radiation. Radiat Prot. Dosimetry **82**: 125–131.

Cheng, X., Pantelias, G. E., Okayasu, R., Cheong, N., and Iliakis, G. 1993. Mitosis-promoting factor activity of inducer mitotic cells may affect radiation yield of interphase chromosome breaks in the premature chromosome condensation assay. Cancer Res. **53**: 5592–5596.

Cornforth, M. N. and Bedford, J. S. 1983. High-resolution measurement of breaks in prematurely condensed chromosomes by differential staining. Chromosoma **88**: 315–318.

Darroudi, F. and Natarajan, A. T. 1993. Premature chromosome condensation, a novel method for biological dosimetry. Proceedings of the 10th International Congress on High Levels of Natural Radiation Vienna, 1993, IAEA, Vienna. pp. 479–485.

Darroudi, F., Fomina, J., Meijers, M., and Natarajan, A. T. 1998. Kinetics of formation of chromosome aberrations in X-irradiated human lymphocytes, using PCC and FISH. Mutat. Res. **404**: 55–65.

Darroudi, F., Bergs, J. V. V., Bezrookove, V., Bist, M. R., Stakoersm K, J., and Franken, N. A. 2010. PCC and COBRA-FISH a new tool to characterize primary cervical carchinomas: to assess hall-marks and stage specificity. Cancer Lett. **287**: 67–74.

Durante, M., George, K., and Yang, T. C. 1997. Biodosimetry of ionizing radiation by selective painting of prematurely condensed chromosomes in human lymphocytes. Radiat. Res. **148**: S45–S50.

Durante, M., Furusawa, Y., and Gotoh, E. 1998. A simple method for simultaneous interphase-metaphase chromosome analysis in biodosimetry. Int. J. Radiat. Biol. **74**: 457–462.

Evans, J. W., Chang, J. A., Giaccia, A. J., Pinkel, D., and Brown, J. M. 1991. The use of fluorescence *in situ* hybridization combined with premature chromosome condensation for the identification of chromosome damage. Br. J. Cancer **63**: 517–521.

Freeman, R. S., and Donoghue, D. J. 1991. Protein kinases and protooncogenes: biochemical regulators of the eukaryotic cell cycle. Biochemistry **30**: 2293–2302.

Garcia, C. L., Carloni, M., Peña, N. P., Jonti, E., and Palitti, F. 2001. Detection of DNA primary damage by premature chromosome condensation in human peripheral blood lymphocytes treated with methyl methanesulfonate. Mutagenesis **16**: 121–125.

Gotoh, E., Tanno Y., and Takakura, K. 2005. Simple biodosimetry method for use in cases of high-dose radiation exposure that scores the chromosome number of Giemsa-stained drug-induced prematurely condensed chromosomes (PCC). Int. J. Radiat. Biol. **81**: 33–40.

Gotoh, E., and Durante, M. 2006. Chromosome condensation outside of mitosis: mechanisms and new tools. J. Cell Physiol. **209**: 297–304.

Gotoh, E. 2007. Visualizing the dynamics of chromosome structure formation coupled with DNA replication. Chromosoma **116**: 453–462.

Gotoh, E. 2009. Drug-induced premature chromosome condensation (PCC) protocols: cytogenetic approaches in mitotic chromosome and interphase chromatin. Methods Mol. Biol. **523**: 83–92.

Hittelman, W. N., Broussard, L. C., and McCredie, K. 1979. Premature chromosome condensation studies in human leukemia. I. Pretreatment characteristics. Blood **54**: 1001–1014.

Hittelman, W. N., Petkovic, I., and Agnor, P. 1988. Improvements in the premature chromosome condensation technique for cytogenetic analysis. Cancer Genet. Cytogenet. **30**: 301–312.

IAEA (International Atomic Energy Agency). 2001. Cytogenetic analysis for radiation dose assessment. A manual. Technical Report Series No. 405. IAEA, Vienna.

IAEA. 2012. Cytogenetic dosimetry: applications in preparedness for and response to radiation emergencies. IAEA, Vienna.

Johnson, R. T., and Rao, P. N. 1970. Mammalian cell fusion: induction of premature chromosome condensation in interphase nuclei. Nature **226**: 717–722.

Kanda, R., Hayata, I., and Lloyd, D. C. 1999. Easy biodosimetry for high-dose radiation exposure using drug-induced, prematurely condensed chromosomes. Int. J. Radiat. Biol. **75**: 441–446.

Lamadrid, A. L., Garcia, O., Delbos, M., Voisin, P., and Roy, L. 2007. PCC-ring induction in human lymphocytes exposed to gamma and neutron irradiation. J. Radiat. Res. **48**: 1–6.

Lindholm, C., Stricklin, D., Jaworska, A., Koivistoinen, A., Paile, W., Arvidsson, E., Deperas-Standylo, J. and Wojcik, A. 2010. Premature chromosome condensation (PCC) assay for dose assessment in mass casualty accidents. Radiat. Res. **173**: 71–78.

M'kacher, R., Violot, D., Aubert, B., Girinsky, T., Dossou, J., Béron-Gaillard, N., Carde, P and Parmentier, C. 2003. Premature chromosome condensation associated with fluorescence *in situ* hybridization detects cytogenetic abnormalities after a CT scan: Evaluation of the low-dose effect. Radiat. Protect. Dosimetry **103**: 35–40.

Nurse, P. 1990. Universal control mechanism regulating onset of M-phase. Nature **344**: 503–508.

Pantelias, G. E., and Maillie, H. D. 1983. A simple method for premature chromosome condensation induction in primary human and rodent cells using polyethylene glycol. Somatic Cell Genet. **9**: 533–547.

Pantelias, G. E., and Maillie, H. D. 1984. The use of peripheral blood mononuclear cell prematurely condensed chromosomes for biological dosimetry. Radiat. Res. **99**: 140–150.

Pantelias, G. E., and Maillie, H. D. 1985. Direct analysis of radiation induced chromosome fragments and rings in unstimulated human peripheral blood lymphocytes by means of the premature chromosome condensation technique. Mutat. Res. **149**: 67–72.

Pantelias, G. E., Iliakis, G. E., Sambani, C. D., and Politis, G. 1993. Biological dosimetry of absorbed radiation by C-banding of interphase chromosomes in peripheral blood lymphocytes. Int. J. Radiat. Biol. **63**: 349–354.

Pathak, R., Ramakumar, A., Subramanian, U., and Prasanna, P. G. S. 2009. Differential radio-sensitivities of human chromosomes 1 and 2 in interphase- and metaphase-spreads after ^{60}Co gamma-irradiation in one human donor. BMC Med. Phys. **9**: 1–9.

Prasanna, P. G. S., Kolanko, C. J., Gerstenberg, H. M., and Blakely, W. F. 1997. Premature chromosome condensation assay for biodosimetry: Studies with fission neutrons. Health Phys. **72**: 594–600.

Prasanna, P. G. S., Escalada, N. D., and Blakely, W. F. 2000. Induction of premature chromosome condensation by a phosphatase inhibitor and a protein kinase in unstimulated human peripheral blood lymphocytes: a simple and rapid technique to study chromosome aberrations using specific whole-chromosome DNA hybridization probes for biological dosimetry. Mutat. Res. **466**: 131–141.

Prasanna, P. G. S., and Blakely, W. F. 2004. Premature chromosome condensation in human resting peripheral blood lymphocytes for chromosome aberration analysis using specific whole-chromosome DNA hybridization probes. In: Keohavong, P., Grants and S. G. (eds.) Methods in Molecular Biology. Vol. 291. Methods in Molecular Biology, Humana Press, Totowa, pp. 49–57.

Prasanna, P. G. S., and Blakely, W. F. 2005. Premature chromosome condensation in human resting peripheral blood lymphocytes for chromosome aberration analysis using specific whole-chromosome DNA hybridization probes. Methods Mol. Biol. **291**: 49–57.

Rao, P. N., and Johnson, R. T. 1970. Mammalian cell fusion: studies on the regulation of DNA synthesis and mitosis. Nature **225**: 159–164.

Rao, P. N., Wilson, B., and Puck. T. T. 1977. Premature chromosome condensation and cell cycle analysis. J. Cell. Physiol. **91**: 131–141.

Slijepcevic, P., Xiao, Y., Natarajan, A. T., and Bryant, P. E. 1997. Instability of CHO chromosomes containing interstitial telomeric sequences originating from Chinese hamster chromosome 10. Cytogenet. Cell Genet. **76**: 58–60.

Sperling, K., and Rao, P. N. 1974. The phenomenon of premature chromosome condensation: its relevance to basic and applied research. Human Genet. **23**: 235–258.

Stevens, J. B., Abdallah, B. Y., Regan, S. M., Liu, G., Bremer, S. W., and Ye, C. J. 2010. Comparison of mitotic cell death by chromosome fragmentation to premature chromosome condensation. Mol. Cytogenet. **3**: 20 (Open access article).

Suto, Y., Hirai, M. Akiyama, M., Suzuki, T., and Sugiura, N. 2012. Sensitive and rapid detection of centromeric alphoid DNA in human metaphase chromosomes by PNA fluorescence *in situ* hybridization and its application to biological radiation dosimetry. Cytologia **77**: 261–267.

Terzoudi, G. I., and Pantelias, G. E. 2006. Cytogenetic methods for biodosimetry and risk individualization after exposure to ionizing radiation. Radiat. Prot. Dosimetry **122**: 513–520.

Terzoudi, G. I., Singh, S. K., Pantelias, G. E., and Iliakis, G. 2008. Premature chromosome condensation reveals DNA-PK independent pathways of chromosome break repair. Int. J. Oncol. **33**: 871–879.

Vyas, R. C., Darroudi, F., and Natarajan, A. T. 1991. Radiation-induced chromosomal breakage and rejoining in interphase-metaphase chromosomes of human lymphocytes. Mutat. Res. **249**: 29–35.

Waldren, C. A., and Johnson, R. T. 1974. Analysis of interphase chromosome damage by means of premature chromosome condensation after X and UV irradiation. Proc. Natl. Acad. Sci. USA **71**: 1137–1141.

Xu, X., Nagarajan, H., Lewis, N. E., Pan S., Cai, Z., Liu, X., Chen, W., Xie, M., Wang, W., Hamond, S., Anderson, M. R., Neff, N., Passarelli, B., Koh, W., Fan, H. C., Wang, J., Gui, Y., Lee, K. H., Betenbaugh, M. J., Quake, S. R., Famili, I., Palsson, B. O., and Wang, J. 2011. The genomic sequence of the Chinese hamster ovary (CHO)-K1 cell line. Nature Biotechnol. **29**: 735–741.

ADVANCED MATERIALS
www.advmat.de

Fragmentation of Poly(lactic acid) Nanosheets and Patchwork Treatment for Burn Wounds

Yosuke Okamura, Koki Kabata, Manabu Kinoshita, Hiromi Miyazaki, Akihiro Saito, Toshinori Fujie, Shinya Ohtsubo, Daizoh Saitoh, and Shinji Takeoka**

In the field of nanotechnology, much attention has recently been focused on the fabrication of freestanding ultrathin films (often called nanosheets or nanomembranes). Because of their extremely large surface-area-to-thickness (aspect) ratio of greater than 10^6 (size on the order of a centimeter but only tens of nanometers thick) the sheets have unique properties, such as high levels of flexibility and adhesiveness.[1,2] The approaches that have been adopted to fabricate these sheets include the use of polymers and/or inorganic nanomaterials such as layer-by-layer (LbL) films of polyelectolytes,[2a–c] assemblies of triblock copolymers,[2d] cross-linked amphiphilic Langmuir–Blodgett films,[2e,f] cross-linked self-assembled monolayers (SAMs),[2g] and densely interpenetrating hybrid network nanomembranes.[2h] These systems have been developed for use in a wide variety of fields, such as nanoseparation membranes or nanosensors for electrochemical and photochemical applications.

For biomedical applications, we recently succeeded in fabricating a freestanding biocompatible polysaccharide nanosheet composed of chitosan and sodium alginate.[3] We also fabricated a series of nanosheets with versatile biodegradable polyesters such as poly(L-lactic acid) (PLLA), poly(glycolide), and their copolymers,[4] which have been clinically used in surgery as degradable sutures,[5a] bone screws, pins, and plates.[5b] These polyesters have also been widely investigated as potential drug carriers.[5c] Thus, the development of nanosheets composed of polyester materials is likely to be the quickest route to successful clinical applications of this new technology. Recently, we have proposed the clinical use of freestanding biodegradable PLLA nanosheets, which have interesting features such as good adhesiveness, exquisite flexibility, and a high level of transparency.[4a] The nanosheet can be used for sealing wounds or suture ligation or their supports during surgery.[4a] Moreover, such a wound repair site showed neither scars nor tissue adhesion.[4a] However, these nanosheets are only suitable for sealing relatively flat and broad interfaces.

A burn wound is a complex and evolving injury. Extensive burn injuries produce, in addition to local tissue damage, systemic consequences.[6] In the management of burn wounds, much attention should be paid to minimizing the risk of burn wound infection during wound healing. Otherwise, superficial and partial thickness wounds often deteriorate into deeper tissue damage. Severe sepsis resulting from burn wound infection is considered to be one of the most critical complications because of its associated high mortality rate. A wide variety of wound dressings is currently available for the treatment of partial thickness burn wounds.[6a] Although such conventional dressings appear to be suitable for wrapping relatively flat interfaces, it is often difficult to efficiently wrap burn wounds with an irregular (not flat) shape such as those associated with fingers, toes, and the perineum.

In this Communication, we propose i) a one-pot fabrication of freestanding biodegradable nanosheets composed of PLLA, ii) their fragmentation, and iii) a simple patchwork technique using the fragmented nanosheets to effectively wrap different shaped materials. Furthermore, we demonstrate that the fragmented PLLA nanosheets act as a physical barrier against burn wound infection with *Pseudomonas aeruginosa*.

Initially, we fabricated a large number of freestanding PLLA nanosheets in one pot, as shown in **Figure 1**A. A 100 mg mL^{-1} solution of poly(vinyl alcohol) (PVA) as a water-soluble sacrificial film was dropped on a SiO_2 substrate and then spin-coated at 4000 rpm for 20 s, followed by drying at 70 °C for 90 s. Next, a 10 mg mL^{-1} solution of PLLA was dropped on the substrate previously coated with PVA, spin-coated (4000 rpm, 20 s) and then dried (70 °C, 90 s). The surface of the substrate was light red in color, and the thickness of the PLLA nanosheet was 60 ± 6 nm. We previously reported that the nanosheets have a high affinity to adhere to a wide range of bio-interfaces.[4a] Hence,

Dr. Y. Okamura, K. Kabata, A. Saito, Dr. T. Fujie, Prof. S. Takeoka
Department of Life Science and Medical Bioscience
Graduate School of Advanced Science and Engineering
Waseda University
TWIns, 2-2 Wakamatsu-cho, Shinjuku-ku
Tokyo, 162-8480, Japan
E-mail: y.okamura@tokai-u.jp; takeoka@waseda.jp
Dr. Y. Okamura
Institute of Innovative Science and Technology
Tokai University
4-1-1 Kitakaname, Hiratsuka, Kanagawa, 259-1292, Japan
Dr. M. Kinoshita
Department of Immunology and Microbiology
National Defense Medical College
Tokorozawa, Saitama, 359-8513, Japan
Dr. H. Miyazaki, Prof. D. Saitoh
Division of Traumatology
National Defense Medical College
Tokorozawa, Saitama, 359-8513, Japan
Dr. S. Ohtsubo
Project Research Institutes
Comprehensive Research Organization
Waseda University
Shinjuku-ku, Tokyo, 162-0041, Japan

DOI: 10.1002/adma.201202851

ADVANCED MATERIALS
www.advmat.de

Materials Views
www.MaterialsViews.com

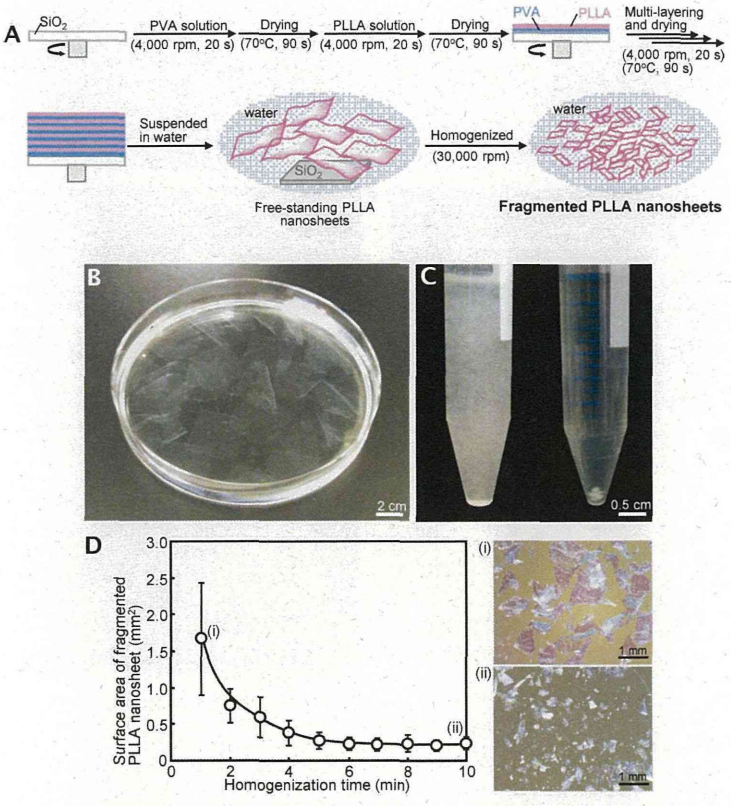

Figure 1. Fabrication and characterization of fragmented PLLA nanosheets. A) Preparation scheme of fragmented PLLA nanosheets by a simple combination of processes. (Process 1: One-pot fabrication of freestanding PLLA nanosheets by a spin-coating-assisted multi-layering/drying of PLLA and PVA and novel peeling technique. Process 2: Homogenization for fragmentation of nanosheets.) B) Macroscopic image of 25 PLLA nanosheets with a thickness of 60 ± 6 nm suspended in water, corresponding to the number of multi-layering processes of PVA and PLLA. C) Macroscopic images of the fragmented PLLA nanosheets (left) and granular PLLA (right) after homogenization at 30000 rpm for 10 min. D) Correlation of the single-side surface area of one fragmented PLLA nanosheet with homogenization time. As a reference, the surface area before homogenization was 1600 mm^2 (40 mm × 40 mm). The experiment was performed at least three times. Values are given as the mean ± SD (standard deviation). Insets i) and ii):Representative images of fragmented PLLA nanosheets adhered on the SiO_2 substrate after 1 and 10 min homogenization, respectively.

the resulting nanosheet with a thickness of less than 100 nm could efficiently cover the interface because of its extreme flexibility, high smoothness, and large contact area.[4a] Subsequently, the multi-layering and the 70 °C drying processes of PVA and PLLA were repeated 25 times on a SiO_2 substrate. By dissolution of the sacrificial PVA layers between PLLA layers or on the substrate in distilled water, we successfully obtained 25 freestanding PLLA nanosheets, corresponding to the number of multi-layering processes of PVA and PLLA (Figure 1B). The resulting nanosheets maintained the shape and size of the SiO_2 substrate (40 mm × 40 mm) and were transparent and extremely flexible (Movie S1, Supporting Information). Consequently, we succeeded in radically improving the productivity of freestanding PLLA nanosheets by a simple combination of a spin-coating-assisted multi-layering process of PVA and PLLA with a peeling technique.

When the suspension of the PLLA nanosheets (single-side surface area of PLLA nanosheet: 1.6×10^3 mm^2) was homogenized at 30000 rpm, they were instantly fragmented. The single-side surface area of one fragmented PLLA nanosheet was significantly decreased with increasing homogenization time and reached a minimum at 0.24 ± 0.08 mm^2 at 7 min (Figure 1D). We noticed that the turbidity and viscosity of the resulting suspension increased with continuing homogenization (Figure 1C, left, and Movie S2, in the Supporting Information). By contrast, however, the commercially available PLLA itself was instantly precipitated when homogenized under the same conditions and became granular PLLA with diameters of approximately 1 mm (Figure 1C, right, and Movie S3, in the Supporting Information). Taking into account the volume (1.44×10^{-14} m^3) and total surface area (4.80×10^{-7} m^2) of the fragmented PLLA nanosheets and the density of PLLA (1.27×10^6 g m^{-3}),[7] a simple calculation gives the specific surface area of fragmented PLLA nanosheets to be 26 m^2 g^{-1}, corresponding to that of nanoparticles with a diameter of 200 nm (24 m^2 g^{-1}). However, the PLLA nanoparticles with comparable diameters adhered on the SiO_2 substrate were easily removed from the substrate by simply washing with distilled water (Figure S1A, Supporting Information), whereas the fragmented nanosheets were difficult to detach even after fragmentation (Figure S1B, Supporting Information). This observation indicates that the nanoparticles, which are being considered as drug delivery carriers for wounds, may not adhere appropriately to the interfaces owing to their small contact area, and the nanosheets, with similarly surface area but enhanced adhesion properties, may be more appropriate for these applications. This is a characteristic feature of nanosheets. The specific surface area of granular PLLA after homogenization (ca. 1 mm diameter) was calculated to be 0.0047 m^2 g^{-1}, assuming the PLLA is made up of spherical particles. Consequently, the specific surface area of fragmented nanosheets was 5500 times that of the granular PLLA.

As described above, the resulting fragmented PLLA nanosheets can be utilized as a suspension (Figure 1C, left, and Movie S2, in the Supporting Information). We have previously reported that PLLA nanosheets float on distilled water without any stabilizers because of their hydrophobic properties.[4a] Interestingly, however, the fragmented nanosheets can be suspended in their open conformation and do not aggregate by hydrophobic interactions in distilled water, even in the absence of any stabilizers. Fourier transform infrared (FTIR) analysis of

the fragmented PLLA nanosheets revealed a band at 3350 cm^{-1}, corresponding to the O–H stretching vibration mode (Figure S2, Supporting Information). This observation suggested that PVA, which is used as a water-soluble sacrificial layer, could be deposited onto the surface of the fragmented PLLA nanosheets during the drying process at 70 °C to help stabilize the suspension. Furthermore, the fragmented PLLA nanosheets can be lyophilized and stably resuspended in distilled water, thereby facilitating their long-term storage as a lyophilized powder (Figure S3, Supporting Information).

Next, we explored the adhesion behavior of the fragmented PLLA nanosheets. The nanosheets were cast on the bare SiO_2 substrate and dried in a desiccator overnight. Intriguingly, the fragmented PLLA nanosheets firmly adhered onto the substrate in a spread-out conformation (i.e., not aggregated or curled up) even in the absence of adhesive reagents (**Figure 2**Ai). Once the nanosheets had dried onto the surface, they were difficult to detach even by scratching with tweezers. The distribution of the nanosheets resembled a "patchwork", which was evident as a sequential series of structural colors on the SiO_2 substrate (Figure 2Aii). The colors depended on the number of overlaid nanosheets according to thin-film interference theory:[3b] red for a single layer (thickness: ca. 60 nm), blue for double layers (ca. 120 nm), and yellow-green for triple layers (ca. 180 nm) (compared with bronze-yellow for the bare SiO_2 substrate at an observation angle of ca. 85°). Some gray lines were also observed in regions of the patchwork. Based on scanning electron microscopy (SEM) observations, these gray areas correspond to wrinkles (not cracks) formed during the adsorption process (Figure 2Aiii). If there were any spaces between the nanosheets (air, etc.), the structural colors as described above would not be observed (i.e., gray color only). These results indicate that the fragmented nanosheets consist of a patchwork, where the sheets are strongly adhered to each other in a spread-out arrangement. In fact, when fragmented PLLA nanosheets at a concentration above 1×10^5 sheets mL^{-1} were cast on a poly(tetrafluoroethylene) (PTFE) plate, which has a lower surface energy than the SiO_2 substrate, the sheets could be detached from the plate as a film picked up with tweezers (Figure 2B). Hence, the fragmented PLLA nanosheets after casting can be reconstructed as one nanosheet on the substrate. Moreover, we investigated the coating properties of the nanosheet by first labeling it with octadecylrhodamine. Using a vertical dipping and lifting method we were able to demonstrate by fluorescence stereomicroscopy that the labeled fragmented nanosheets efficiently coat several different interfaces, such as an 18 gauge (18G) needle (steel), a human skin model

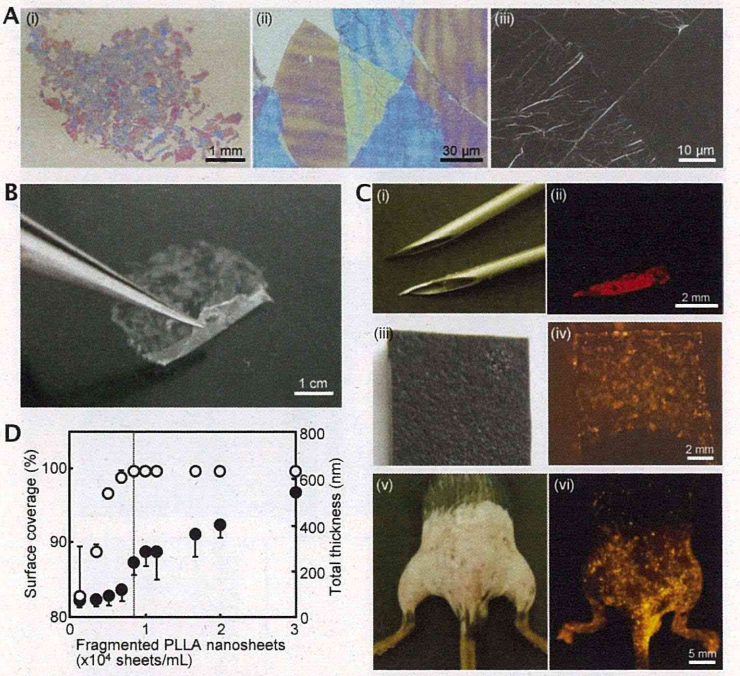

Figure 2. Patchwork of fragmented PLLA nanosheets on several interfaces. A) Macroscopic (i) and microscopic (ii,iii) images of fragmented PLLA nanosheets adhered on the SiO_2 substrate obtained using a digital camera, a digital microscope, and a scanning electron microscope, respectively. B) Detachment of fragmented PLLA nanosheets from the PTFE plate. This result indicates that the fragmented PLLA nanosheets can be reconstructed as one film after casting. C) Ubiquitous patchwork of the fragmented PLLA nanosheets labeled with octadecylrhodamine on the irregularly shaped interfaces (18G needles (i,ii), the lower needle in each case is coated with the nanosheets and the upper one not; artificial skin derived from polyurethane resin (iii,iv); and mouse skin (v,vi)) by a vertical dipping and lifting method. Odd- and even-numbered images were taken under visible light and in the fluorescence mode, respectively. D) Correlation of surface coverage (empty circles) and thickness (filled circles) of fragmented PLLA nanosheets on SiO_2 substrate with their concentration. The experiment was performed at least three times. Values are given as the mean ± SD.

derived from polyurethane resin (plastics), and the lower half of the mouse body, including the perineum, which constitutes an irregular shape (Figure 2C). The nanosheets were barely detectable under visible light, indicating that the ultrathin and flexible fragmented nanosheets adhered along the roughness of the interfaces at the nanometer scale. This is a noteworthy characteristic of nanosheets generated using the patchwork technique when adhered to an irregular surface.

Next, we determined the optimal amount of fragmented PLLA nanosheets for generating a patchwork. When 50 μL of the nanosheet suspension with different concentrations of less than 8.3×10^3 sheets mL^{-1} was cast on the SiO_2 substrate (6 mm × 6 mm: 36 mm^2) as a model interface, the nanosheets were randomly adsorbed on the substrate in a spread-out manner as described above (Figure S4, Supporting Information). With increasing concentration of the nanosheet suspension (1.0, 3.3, 5.0, and 6.7×10^3 sheets mL^{-1}), the surface coverages (83 ± 7, 89 ± 1, 97 ± 1, and 99 ± 1%, respectively) and average thicknesses (74 ± 29, 79 ± 31, 99 ± 44 and 124 ± 52 nm,

ADVANCED MATERIALS
www.advmat.de
www.MaterialsViews.com

respectively) of the patchwork gradually increased (Figure 2D). However, the coverage did not reach 100%, although portions of the nanosheets started to be overlaid with each other. At 8.3×10^3 sheets mL^{-1}, the coverage did reach 100% and the average thickness of adhered nanosheets was calculated to be 244 ± 56 nm, corresponding to 3–5 layers of fragmented nanosheets (Figure 2D). Above this concentration, the surface coverage was maintained at 100% and the thicknesses of the resulting nanosheets increased proportionally. Based on these measurements we calculated that 415 fragmented nanosheets, which had a total single-side surface area of approximately 100 mm^2, were applied to a SiO_2 substrate to cover an area of 36 mm^2. Consequently, we judged that a perfect patchwork could be achieved by applying a three-fold excess of single-side surface area of nanosheets over that of the desired patchwork surface area.

Subsequently, we evaluated whether the patchwork of fragmented PLLA nanosheets could act as a practical physical barrier against burn wound infection. *P. aeruginosa* is a common cause of such infections. Initially, we tested the ability of the patchwork to form an effective seal by using a bacterial permeability assay on a Transwell Membrane (TM, diameter: 6.5 mm) kit (**Figure 3**A). The fragmented PLLA nanosheets (8.3×10^3 sheets mL^{-1}, 50 µL) were allowed to adhere on the surface of the TM under the conditions required for the perfect patchwork as described above. Interestingly, microscopic observations of the surface of the TM revealed that the fragmented nanosheets could be used to generate a perfect seal to cover not only the intrinsic pores of TM (8 µm diameter) but also additional pores of 1.2 mm diameter, which are much larger than the dimensions of the fragmented nanosheets (Figures 3Bii and iv).

Next, an in vitro bacterial permeability assay was set up using a TM coated with fragmented nanosheets or a control TM (without nanosheets). The number of *P. aeruginosa* passing through the control TM to the outer well was calculated to be $7.7 \pm 1.7 \times 10^6$ CFU (colony forming unit) mL^{-1} 6 h after culturing (Figure 3C). However, the number of bacteria passing through the TM coated with fragmented nanosheets ($0.33 \pm 0.14 \times 10^6$ CFU mL^{-1}) was significantly lower than that of the control TM. The bacterial counts in the inner wells of the nanosheet-coated TM and control TM were similar (i.e., $14.3 \pm 1.5 \times 10^6$ CFU mL^{-1} vs. $11.8 \pm 2.3 \times 10^6$ CFU mL^{-1}, respectively). These results demonstrate that the fragmented nanosheets can form an effective barrier against penetration by *P. aeruginosa*. Taken together, our results indicate that the fragmented nanosheets can be formed into a single nanosheet that acts as a physical barrier to bacterial permeation.

Finally, we studied the in vivo therapeutic barrier effect of the fragmented PLLA nanosheets using a mouse model of superficial dermal burn (SDB)

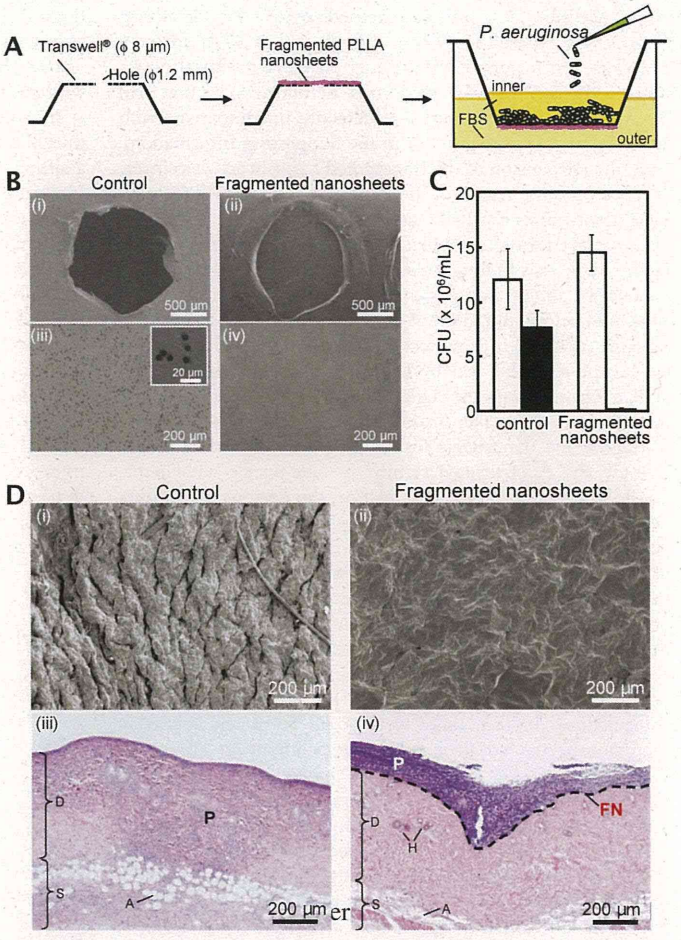

Figure 3. In vitro and in vivo therapeutic barrier effect of the fragmented PLLA nanosheets. A) Schematic illustration of the bacterial permeability assay. The fragmented PLLA nanosheets were coated on a TM with a pore size of 8 µm and three additional larger pores (diameter: 1.2 mm each) to measure the permeability of *P. aeruginosa*. The permeability of *P. aeruginosa* was measured using a 24 Transwell plate 6 h after culturing. FBS: Fetal bovine serum. B) SEM images of TM coated with fragmented PLLA nanosheets (ii,iv) and TM only (i,iii). Images (i) and (ii) show the region around the additional pore, whereas images (iii) and (iv) show the region of the intrinsic pores. Inset in (iii):High-magnification image of (iii). C) In vitro barrier effect of fragmented PLLA nanosheets adhered on the TM. The bacterial cell count in the outer and inner wells was determined after 6 h and is represented by the black and white columns, respectively. The experiment was performed at least three times. Values are given as the mean ± standard error of mean (SE). D) In vivo therapeutic barrier assay. i,ii) SEM images of SDB-induced skin injury before (i) and after (ii) patchwork treatment with the fragmented nanosheets. This observation shows that the fragmented nanosheets could wrap the uneven skin with SDB-induced injury. iii,iv) Histological images stained with H&E, showing the skin with SDB-induced injury without (iii) or with (iv) the nanosheet-patchwork. The skin samples were taken from the mice 3 days after the application of *P. aeruginosa*. Image (iii) shows that the *P. aeruginosa* stained in blue-purple infiltrated both the dermis and subcutaneous layer (compared to Figure S5B (Supporting Information): the skin with SDB-induced injury before application of the nanosheets and the *P. aeruginosa*). Image (iv) shows that the *P. aeruginosa* remained on the surface of the nanosheets, as depicted by the dashed line, yielding an excellent barrier effect by the patchwork treatment. The letters A, D, FN, H, P, and S in the histological images indicate adipose tissue, dermis, fragmented nanosheets, hair root, *P. aeruginosa*, and subcutaneous layer, respectively.